Graphene-Patched CNT/MnO₂ Nanocomposite Papers for the Electrode of High-Performance Flexible Asymmetric Supercapacitors

Yu Jin,[†,‡,§] Hongyuan Chen,[†,§] Minghai Chen,*[,†] Ning Liu,[‡] and Qingwen Li*[,†]

[†]Suzhou Institute of Nano-tech and Nano-bionics, Chinese Academy of Sciences, Suzhou 215123, People's Republic of China
[‡]School of Materials Science and Engineering, Hefei University of Technology, Hefei 230009, People's Republic of China

Ⓢ *Supporting Information*

ABSTRACT: MnO₂ has been widely studied as the pseudo-capacitive electrode material of high-performance super-capacitors for its large operating voltage, low cost, and environmental friendliness. However, it suffers from low conductivity and being hardly handle as the electrodes of supercapacitors especially with flexibility, which largely limit its electrochemical performance and application. Herein, we report a novel ternary composite paper composed of reduced graphene sheet (GR)-patched carbon nanotube (CNT)/ MnO₂, which has controllable structures and prominent electrochemical properties for a flexible electrode of the supercapacitor. The composite paper was prepared by electrochemical deposition of MnO₂ on a flexible CNT paper and further adsorption of GR on its surface to enhance the surface conductivity of the electrode and prohibit MnO₂ nanospheres from detaching with the electrode. The presence of GR was found remarkably effective in enhancing the initial electrochemical capacitance of the composite paper from 280 F/g to 486.6 F/g. Furthermore, it ensures the stability of the capacitance after a long period of charge/discharge cycles. A flexible CNT/polyaniline/CNT/MnO₂/GR asymmetric supercapacitor was assembled with this composite paper as an electrode and aqueous electrolyte gel as the separator. Its operating voltage reached 1.6 V, with an energy density at 24.8 Wh/kg. Such a composite structure derived from a multiscale assembly can offer not only a robust scaffold loading MnO₂ nanospheres but also a conductive network for efficient ionic and electronic transport; thus, it is potentially promising as a novel electrode architecture for high-performance flexible energy storage devices.

KEYWORDS: carbon nanotube, MnO₂, graphene, buckypaper, supercapacitor
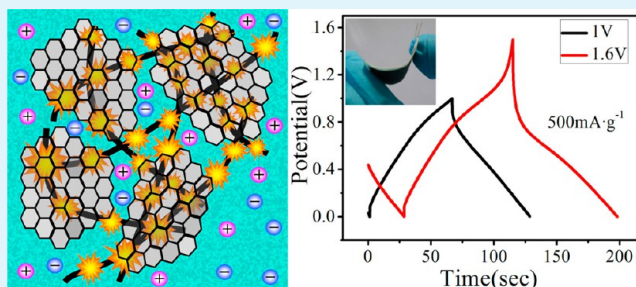
1. INTRODUCTION

Nowadays, the popularization of commercialized pocket electronic devices, such as wearable or foldable electronics, smart products, electronic papers, and mobile electronic devices, makes the development of inexpensive, flexible, lightweight, and environmentally friendly energy storage devices a priority.[1] Among these devices, electrochemical capacitors (ECs, also called supercapacitors) have attracted increased attention, because of their high power density, high charge/discharge rates, and long cycle lifetime.[2−4] However, the low energy density of ECs has limited their application in commercialized devices.[5] Compared to carbon electrode materials for electrochemical double-layer capacitors,[6] pseudo-capacitive electrode materials including transition-metal oxides and conductive polymers have larger electrochemical capacitances and energy densities and, therefore, could satisfy the needs of high-performance supercapacitors.[7]

Among the various pseudo-capacitive materials, manganese dioxide, (MnO₂) has attracted much attention for its good electrochemical capacitive properties, wide potential range, low cost, and environmental friendliness.[2] However, it suffers from inherent drawbacks, because its low electrical conductivity $(10^{-5}-10^{-6}$ S/cm) and the cycling crystal shrinkage/expansion

induced flaking off[8] during the charge/discharge process, which resulted in its practical specific capacitance and cycling stability far below theoretical values. Wrapping MnO₂ onto a conductive network could repair these shortages, to a certain extent. Some conductive scaffolds such as carbon fiber paper,[9] active carbon textile,[10] conductive cotton textile,[11−13] and nickel form,[14,15] were used to load MnO₂, with the objective of increasing electrode conductivity and restricting its volume change. However, the mass loading of MnO₂ on these scaffolds was far from the commercial level for their small specific area. Furthermore, the active materials could be easily detached from the scaffold in the charge/discharge process. Freestanding carbon nanotube (CNT) paper was proposed as flexible paper-like electrode for supercapacitors. Its porous network structure with highly electrical conductivity is beneficial for both the diffusion of electrolytes and the increase of electrical conductivity in the electrode. Furthermore, it affords a platform for mass loading of active materials.[16] The mass loading of MnO₂ in CNT paper could construct a flexible paper-like

electrode material.[17] However, the MnO$_2$ nanostructure coated on CNTs could not form a tight bonding, because of its polycrystalline structure,[18] and the collapsed MnO$_2$ crystal was likely to detach from CNT networks during the electrochemical charge/discharge process, thus resulting in bad cycling performance. In addition, the MnO$_2$ coating would dramatically decrease the surface conductivity of the electrode. Consequently, if another conductive layer can be wrapped around them, these problems can be effectively resolved. Single-walled CNTs and conductive polymers have already been introduced on the surface of MnO$_2$ nanoflowers with largely enhanced electrochemical performances.[19] Actually, considering the prominent advantages in conductivity and stability, reduced graphene sheet (GR) is a more suitable candidate for conductive coating materials, compared with conductive polymers.[20] CNT paper-based electrodes could easily achieve this compound structure by soaking it in GR solution without structure collapse.

In this paper, a freestanding and flexible ternary CNT/MnO$_2$/GR composite paper with a novel structure was prepared by a multistep strategy and introduced as an electrode for constructing flexible supercapacitor. MnO$_2$ nanostructure with controllable morphologies was electrochemically decorated on the flexible CNT paper. Afterward, another GR layer was patched on the surface of the composite paper by a soaking method, with the objective of preventing MnO$_2$ nanospheres from detaching with the CNT "caudexes" and increasing the surface conductivity of the paper as well. The composite electrode shows a higher electrochemical capacitance and better cycling stability than the system without the GR sheet. Furthermore, a flexible asymmetric supercapacitor composed of this electrode and another electrode composed of CNT paper coated by polyanilin (PANI) shows a high energy density, with an operating voltage of 1.6 V.

2. EXPERIMENTAL SECTION

Materials. Multiwalled CNTs (MWCNTs) were synthesized by a floating catalyst chemical vapor deposition (CVD) method. Graphene oxide was prepared using Hummer's method and reduced according to the literature, with the purpose of obtaining a highly conductive GR nanosheet.[21,22] Manganese sulfate (MnSO$_4 \cdot$H$_2$O), sulfuric acid (H$_2$SO$_4$), potassium hydroxide (KOH), aniline, hydrochloric acid (HCl), sodium sulfate (Na$_2$SO$_4$), polyvinylpyrrolidone (PVP K-30), acetone, and Tween-80 were of analytical grade and purchased from Sinopharm Chemical Reagent Co., Ltd. (Shanghai, PRC). The cellulose filter membranes with a pore diameter of 0.45 μm were purchased from Hangzhou ANOW Microfiltration Co., Ltd. (Hangzhou, PRC). Deionized water and absolute alcohol were used as the solvent throughout the entire experiment.

Preparation. CNT papers were prepared by a vacuum filtration method. In a typical process, pristine MWCNTs were sheared into "CNT cotton" by high-speed shearing, and then immersed into hydrochloric acid aqueous solution (5 mol/L) for 48 h to remove catalyst particles. The purified MWCNTs were sheared into "CNT cotton" again and dispersed into deionized water by ultrasonic treatment with the help of Tween-80 (as the dispersant). Then, the uniformly dispersed CNT solution was filtered through a microporous cellulose filter membrane, using vacuum filtration, and washed by deionized water repeatedly to remove remnant dispersants. A freestanding CNT paper was obtained after dissolving the

cellulose filter membrane by acetone. The size of the CNT paper was dependent on the size of the filter, which ranged from 40 mm in diameter to A4 scale. This CNT paper showed moderate flexibility and could be rolled or bent (see Figure 1a).
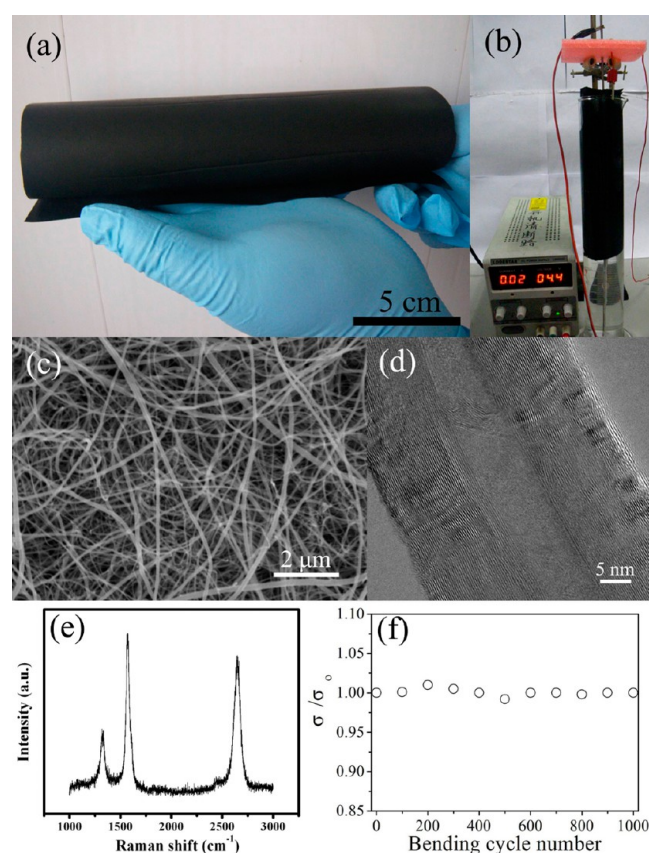

Figure 1. (a) Pristine CNT paper with A4 size; (b) a tube setup used for electrochemical deposition MnO$_2$ on large-size CNT paper; (c) SEM image of pristine CNT paper; (d) TEM image of pristine MWCNT; (e) Raman spectrum of pristine CNT paper; and (f) stable electrical conductivity of pristine CNT paper after cyclic bending.

MnO$_2$ nanoparticles were coated on the CNT papers, using an electrochemical galvanostatic deposition processes with a two-electrode model. For the large area electrochemical deposition, CNT paper was bent into the shape of a ring in a 500-mL graduated cylinder, which was used as the working electrode, and a stainless steel rod was used as the auxiliary electrode (Figure 1b). In addition, the electrolyte was an aqueous solution that consisted of 0.6 M MnSO$_4$ and 0.8 M H$_2$SO$_4$, and the electrochemical deposition temperatures were controlled by a water bath. The as-prepared composite paper was rinsed with deionized water to remove remnant electrolytes. Later, the composite paper was soaked in a GR solution (0.05 mg/mL) for several hours to adsorb GR on its surface. The final product was dried under vacuum at 60 °C for 4 h and collected for the following use. Similarly, as the other electrode of the asymmetric supercapacitor, flexible CNT/PANI composite paper was prepared by cyclic voltammetry (CV) electrochemical polymerization in a mixture electrolyte solution of 1 mol/L H$_2$SO$_4$ and 0.5 mol/L aniline for 300 cycles. A graphite sheet was used as auxiliary electrode and the saturated calomel (SCE) was used as the reference electrode. The voltage window was set at a range of −0.2 V to 0.8 V and the scan rate was 100 mV/s.

Characterization. The mass of MnO_2 on the CNT paper was obtained from weighting the mass change of CNT paper before and after MnO_2 deposition by a high-precision electronic balance. The microstructures of the samples were observed by scanning electron microscopy (SEM) (Quanta 400 FEG, FEI) and transmission electron microscopy (TEM) (Tecnai G2 F20 S-Twin, FEI). The X-ray diffraction (XRD) patterns were obtained using an X'Pert-Pro MPD X-ray diffractometer (PANalytical B.V., The Netherlands). The Raman spectrum was measured by a laser confocal Raman microscopy (LabRAM HR, HORIBA Jobin−Yvon). The sheet resistances of as-prepared paper electrodes were tested by four-probe equipment (Model ST-2258A, Suzhou Jingge Electronic Co., Ltd., China). The mechanical tensile strength was measured by a universal testing machine (Instron 3365) with a load cell of 10 N.

Electrochemical Measurements. The electrochemical measurements were performed using a CHI 660C electrochemical workstation (CH Instruments, Inc., China) interfaced to a computer system with corresponding electrochemical software. The pristine CNT paper was loaded with 5 mg of samples being incorporated into nickel foam (1 cm × 1 cm), which was used as the current collector to prepare the working electrode. The sample was sandwiched between two pieces of nickel foam, and then the sandwich structure was pressed by a hydraulic pressure machine under a pressure of 6 MPa, with the objective of ensuring close contact between the nickel foam and the CNT paper. However, for the sample containing MnO_2, a graphite sheet (2 cm × 6 cm) was used as the current collector. One tip of a composite paper 1 cm × 3 cm in size was adhered onto the surface of the graphite sheet by a carbon black/PTFE gel (prepared with 0.1 mol/L PTFE aqueous solution; the mass ratio of PTFE to carbon black is 1:4), which was usually used as the conductive filler and bond of the commercialized electrochemical electrode for supercapacitor and lithium-ion battery. The adhered tip of the sample was not immersed into the electrolyte in the process of electrochemical performance test. The relative statement has already been inserted into the revised manuscript. The electrochemical properties of the single electrode were tested in aqueous solution as the electrolyte. We used a three-electrode glass cell setup in the experiment, which consisted of a working electrode, a platinum wire as the counter electrode, and a saturated calomel electrode (SCE) as the reference electrode. All potentials reported here have been measured versus SCE. The pristine CNT paper and composite CNT paper were tested in different electrolytes with different potential ranges. Pristine CNT paper was tested in 6 M KOH aqueous solution with a potential range of −1−0 V (vs SCE), while composite CNT paper with MnO_2 or PANI was tested in a 1 M Na_2SO_4 aqueous solution with a potential range of −0.1 V to 0.8 V (vs SCE). The galvanostatic charge/discharge curves were performed at current densities of 0.5, 1, 2, 5, and 10 A/g, respectively. The asymmetric flexible supercapacitor was assembled according to the reported method,[23] using CNT/MnO_2/GR as the positive electrode, CNT/PANI as the negative electrode, and Na_2SO_4/PVP gel as the electrolyte/separator. EIS curves were tested using a CHI660C electrochemical workstation, applying an alternating current in the frequency range from 100 kHz to 10 MHz, with an amplitude of 5 mV.

The specific capacitance of the electrode was calculated from two methods: eq 1 (CV curves) and eq 2 (galvanostatic charge/discharge curves):

$$C = \frac{\int_{V_a}^{V_c} I(V)\, dV}{mv(V_a - V_c)} \quad (1)$$

where C is the specific capacitance (F/g), m is the mass of the electrode (g), v is the scan rate of CV curves (V/s), and $(V_a - V_c)$ represents the potential window (V).

$$C = \frac{I\Delta t}{m\Delta v} \quad (2)$$

where C is the specific capacitance (F/g), I the discharge current (A), m the mass of the electrode (g), ΔV the potential drop (V), and Δt the total discharge time (s).

The energy density (E) and power density (P) of the assembled supercapacitor were calculated from CV curves, according to eqs 3 and 4:

$$E = \frac{1}{2}CV^2 \quad (3)$$

where C is the specific capacitance (F/g), V the potential drop (V), and t the discharge time.

$$P = \frac{E}{t} \quad (4)$$

Here, all of the electrochemical performance values are calculated according to the mass of the entire composite paper electrodes, but not the mass of active materials (such as MnO_2 or GR) on them.

3. RESULTS AND DISCUSSION

Figure 1c shows the surface morphology of the as-prepared CNT paper, which was composed of random MWCNT network with a low stacking density. This porous structure was favorable for active materials loading onto CNT paper by the following electrochemical deposition process. The uniform planar network in this CNT paper is formed by ultralong MWCNTs with a diameter of 50−80 nm and lengths up to hundreds of micrometers. These features are critical for freestanding CNT papers to achieve good flexibility and maintain sufficient porosity. Moreover, the MWCNTs that we used are well-crystallized, as shown in Figure 1d, and the high G/D ratio in the Raman spectrum of MWCNTs (see Figure 1e) further confirms this judgment. This feature could induce the large electrical conductivity of individual CNTs. The electrical conductivity of the pristine CNT paper was measured as 4350 S/m using four-probe equipment, which is much larger than it composed of commercialized MWCNTs (1280 S/m for the CNT paper, produced by MWCNTs purchased from CNano Technology (Beijing), Ltd., PRC). Furthermore, the electrical conductivity of the CNT paper shows negligible variation (Figure 1f) after cycling bending, demonstrating good flexible stability.

MnO_2 was deposited on the CNT paper by the galvanostatic electrochemical deposition process mentioned above. Current density is important for galvanostatic electrochemical deposition. In order to optimize the deposition current, a comparative experiment was first designed with different current densities (1, 3, 5, 7, and 10 mA cm^{-2}) while maintaining the other parameters (deposition time = 1 h, temperature = 75 °C). The as-prepared samples were characterized by XRD and electrochemical capacitance testing. It was found that the current density had no obvious effect on the MnO_2 crystal. In Figure S1a in the Supporting Information, all the diffraction peaks
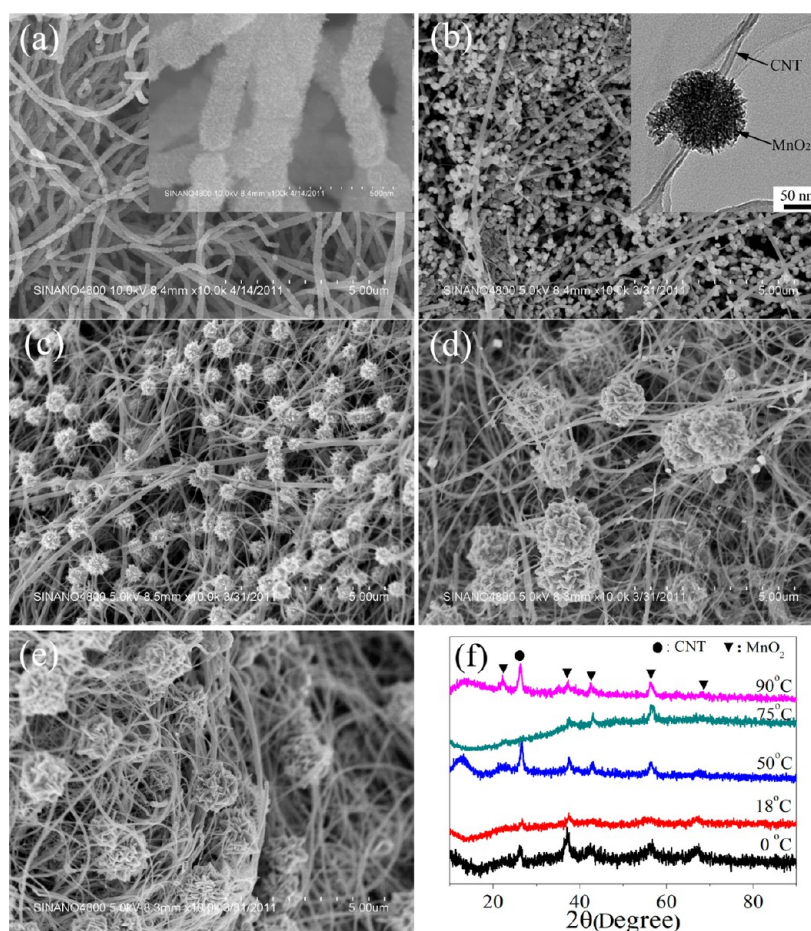
Figure 2. SEM images of the CNT/MnO$_2$ composite prepared at different temperatures: (a) the temperature of water and ice mixture (near to 0 °C), continuous coating (inset shows an SEM image with higher magnification); (b) 18 °C nanospheres (inset shows a TEM image of CNT/MnO$_2$ necklace-like structure); (c) 50 °C, nanoflowers; (d) 75 °C, nanoflowers; (e) 90 °C, nanoflowers; and (f) XRD patterns of composite electrodes prepared at different temperatures.

derived from MnO$_2$ could be indexed to γ-MnO$_2$.[17,24] The ratio curves of specific capacitances versus charge–discharge current density for the CNT-MnO$_2$ composites mass and the pure MnO$_2$ mass are shown in Figures S1b and S1c in the Supporting Information, respectively. It is revealed that 5 mA cm^{-2} is the best current density for achieving good specific capacitance. The calculated specific capacitance, based on the CNT-MnO$_2$ composites mass and pure MnO$_2$ mass, could reach 245 F g^{-1} and 296 F g^{-1}, respectively, under a current density of 100 mA g^{-1}.

The temperature of the galvanostatic electrochemical deposition is an important factor for controlling MnO$_2$ nanostructure coated on CNT paper, sequentially affecting the electrochemical performance of the composite paper. In this study, the temperature was controlled by a water bath, ranging from ice water (0 °C), to room temperature (~18 °C), to hot water (50, 75, 90 °C). It was found that the morphology of the MnO$_2$ differed greatly with the variation of the deposition temperature, as shown in Figures 2a–e. When the temperature of the deposition water bath was decreased close to that of the mixture of ice and water (near to 0 °C), it can be seen that MnO$_2$ nanoflakes are uniformly coated on the surface of CNTs, forming a core/shell cable structure. As the deposition temperature increased, the morphologies of MnO$_2$ varied from nanoflakes to nanospheres (also see Figure S2 in the Supporting Information). Figure 2b shows that a large

number of spherical MnO$_2$ particles were uniformly and discretely attached on the surface of CNTs under a deposition temperature of 18 °C. The close-up TEM image (insert image of Figure 2b) shows that some spherical particles are coated around the CNTs, forming a necklace-like structure. The size of MnO$_2$ nanospheres increases as the deposition temperature increases. Actually, the crystal morphology is affected by many issues, including substrate, supersaturation, ions transportation speed, and so on. In this study, the surface defects on CNTs served as nucleation sites for MnO$_2$ at the early stage. The subsequent growth stage was dominated by the ion deposition speed, which was sensitive to environmental temperature. At low temperatures, the ion concentration around the early nucleated particles was not high enough to achieve critical supersaturation; therefore, the crystal growth speed was very low. It resulted in abundant MnO$_2$ nanoparticles nucleating around CNT to form continuous dense coating. Crystal growth speed could increase as the deposition temperature increases. It would fast consume the ions around them, resulting in fast inhomogeneous growth. Dendritic or hierarchical crystals would dominate the products, just as the MnO$_2$ nanospheres obtained at temperatures higher than 50 °C.

XRD patterns of the corresponding composite papers are shown in Figure 2f. It is found there is no clear change in crystal structure when deposition temperatures were increased. The diffraction peaks at ~22°, 26°, 37.2°, 42.3°, 57.2°, and 66.6° can
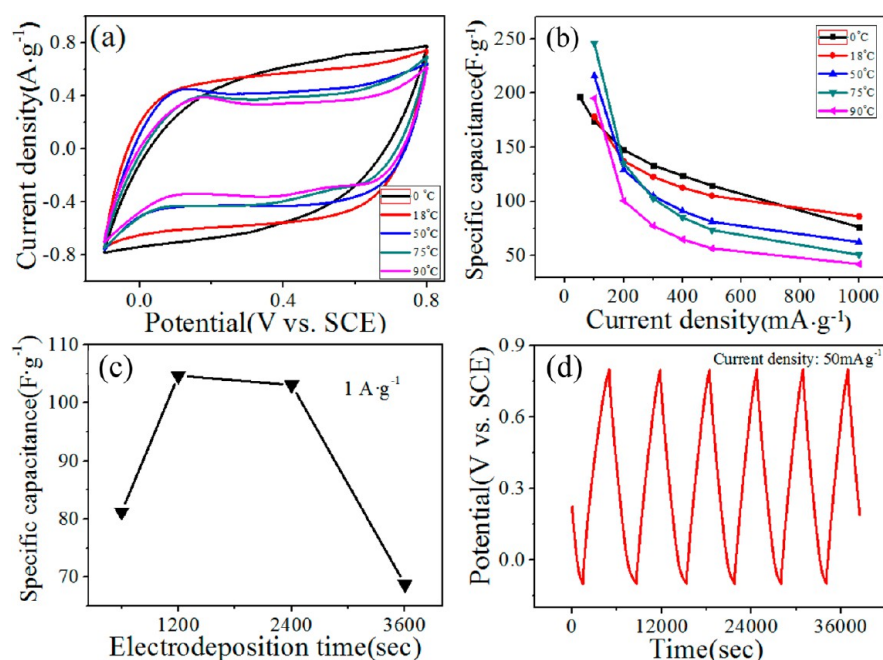
Figure 3. Electrochemical performance of CNT/MnO$_2$ composite papers prepared under different conditions: (a) CV curves (at a scan rate of 5 mV/s) and (b) rate performance of the composite papers prepared at different temperatures; (c) dependence of the specific capacitance of the composite paper on deposition time at a temperature of 18 °C; and (d) typical charge/discharge curve of the sample prepared at room temperature (current density = 50 mA/g).
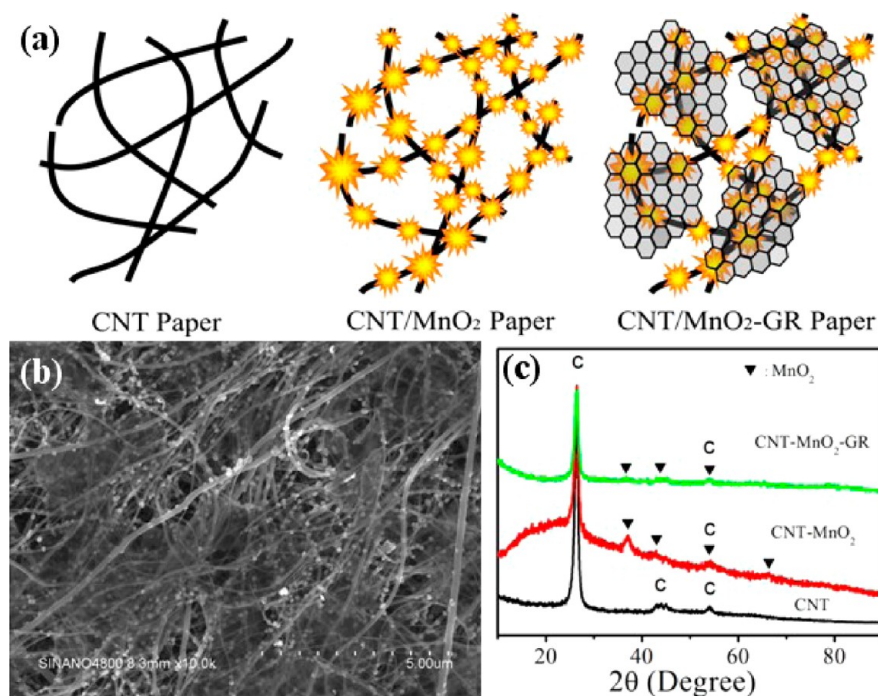

Figure 4. (a) Schematic illustration for the fabrication procedure of CNT/MnO$_2$/GR papers; (b) SEM image of CNT/MnO$_2$/GR paper; and (c) XRD patterns.

be assigned as the crystal planes of (110), (021), (121), (211), and (061) in γ-MnO$_2$ (JCPDS File Card No. 14-644).[17,24] The valence of Mn in the oxide nanostructure could be estimated from XPS spectra as shown in Figure S3 in the Supporting Information. It could be ~4, according to the binding energy of Mn 3s in Figure S3b in the Supporting Information.[25]

Figure 3 shows the electrochemical tests of MnO$_2$/CNT composite paper samples, including CV curves, charge—discharge curves, and rate performance curves of specific capacitance versus current density. Figure 3a shows CV curves (scan rate of 5 mV/s) of CNT/MnO$_2$ composites prepared at different temperatures. It can be seen that all the composite papers show typical square-shaped CV curves, which indicate good supercapacitor behavior. As temperature increased, the current peaks of CV curves were monotonically decreased. Although the sample prepared at a temperature near 0 °C
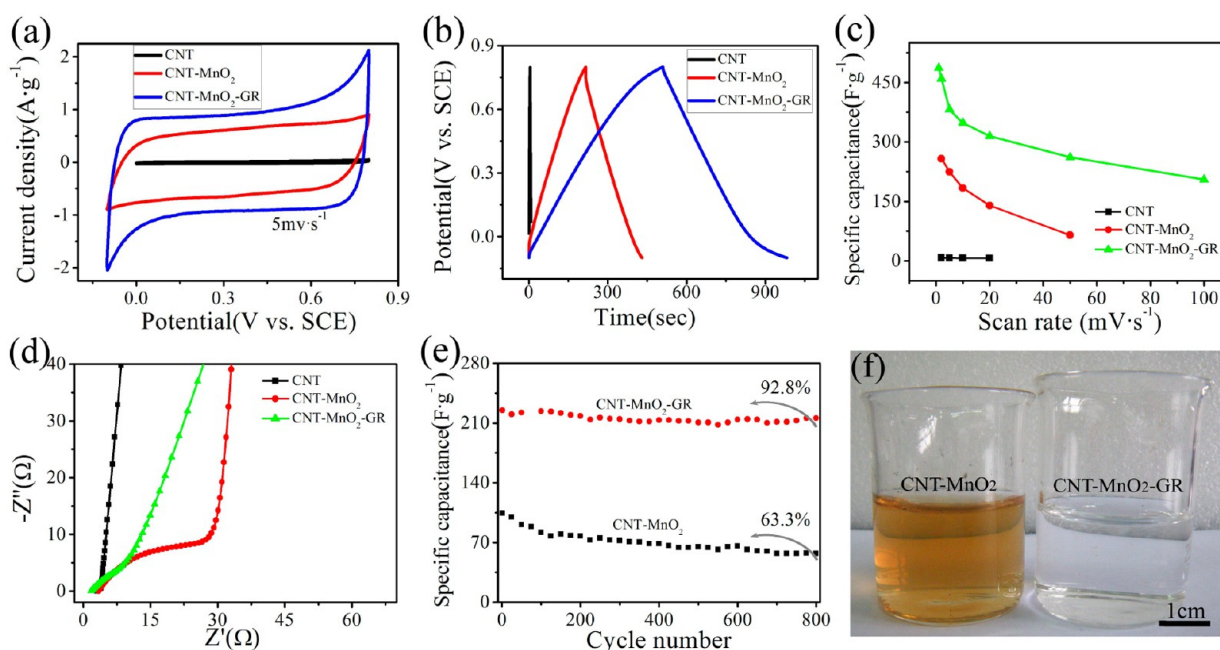
Figure 5. Electrochemical tests: (a) CV curves (5 mV/s); (b) charge/discharge curves (500 mA/g); (c) ratio curves of specific capacitance versus scan rate; (d) Nyquist plots; (e) cycling life test at current density of 1 A/g; and (f) electrolyte solution change after 800 cycles.

shows the highest current peak, the shape of CV curves is far from square. This can be attributed to the poor conductivity by the continuous MnO_2 nanosheet coating around CNTs. The specific capacitance of the samples in Figure 3a can be estimated from the CV curves by integrating the area, and the corresponding results are 177.5 F/g (0 °C), 190.8 F/g (18 °C), 148.6 F/g (50 °C), 129.4 F/g (75 °C), and 118.2 F/g (90 °C), respectively. Figure 3b shows the rate performance curves of specific capacitances versus current density, which indicate that the samples prepared at low temperature (0 and 18 °C) exhibit good high-rate capability. Furthermore, the composite paper deposited at 18 °C shows the highest specific capacitance at large current density (1 A/g), which is consistent with the result of CV curves. Thus, it is reasonable to set the deposition temperature near room temperature (18 °C) to obtain good electrochemical capacitance performance. Further comparative experiments, based on deposition time, were conducted, where the current density (5 mA/cm²) and temperature (18 °C) were kept constant. The corresponding result is shown in Figure 3c, indicating that the specific capacitance (1 A/g) reaches its maximum after 20 min. Further prolonging the deposition time would rapidly deteriorate its specific capacitance. The over-deposition after 20 min would result in many large-sized nanospheres thickly wrapped around CNTs and dramatically decreased the effective surface area and electrical conductivity. Figure 3d is the typical charge and discharge curve of the composite paper prepared at room temperature under the current density of 50 mA/g, which forms a symmetrical triangle and indicates the reversibility of CNT/MnO_2 as an electrode is good.

Based on the above comparative experiments, the deposition parameters were optimized with a current density of 5 mA/cm², a temperature of 18 °C, and a deposition time of 20 min. The mass content of MnO_2 in the composite paper was ~33 wt %. The density of the composite paper was slightly higher than the pristine CNT paper (both ~0.3 g/cm³), with an increase in thickness. The composite electrode prepared under this

condition was compounded with GR as the scheme shown in Figure 4a. After immersion in GR solution for 4 h, the adsorbed GRs were patched on the composite paper's surface to enhance the surface conductivity of the composite paper, and the transparent GR film can be clearly distinguished in Figure 4b as a conductive layer to countervail the low conductivity of MnO_2 nanospheres. The mass of GR sheet on the composite paper is ultrasmall (lower than 1 wt %) and could be ignored. In Figure 4c, the XRD patterns show dominating diffraction peaks from carbon nanomaterials, and the remaining peaks can be indexed to γ-MnO_2. Furthermore, the in-plane electrical conductivity of the composite paper increased from 1.35 S/m to 1.67 S/m after being coated by a GR sheet. It could be a significant benefit for improving the electrochemical performance of the composite paper. The electrical conductivity of the composite paper remained stable in the process after bending 1000 times (see Figure S4 in the Supporting Information), which could indicate the flexibility of the composite paper.

Figure 5a shows CV curves of different composites (CNT paper, CNT/MnO_2, CNT/MnO_2/GR) at a scan rate of 5 mV/ s. The larger loop area of the CV curve indicates the higher specific capacitance. Among the three samples, CNT/MnO_2/ GR shows the highest peak current density and the largest loop area, indicating the largest electrochemical capacitance. Furthermore, its peak current density remains more stable than that of the other two samples in a large potential range. These characteristics indicate the superior capacitive performance of the ternary composite paper. Furthermore, the composite paper shows a stable shape as the scan rate increased from 1 mV/s to 100 mV/s (see Figure S5 in the Supporting Information). It reveals good rate performance, especially at large charge/discharge current densities. Figure 5b shows the charge/discharge curves at the current density of 500 mA/g, and the symmetrical triangle curves indicate the good reversibility of the composite paper electrode. Figure 5c shows the rate performance curves of specific capacitance versus scan rates of CV tests. It indicates that the adsorption of GR on
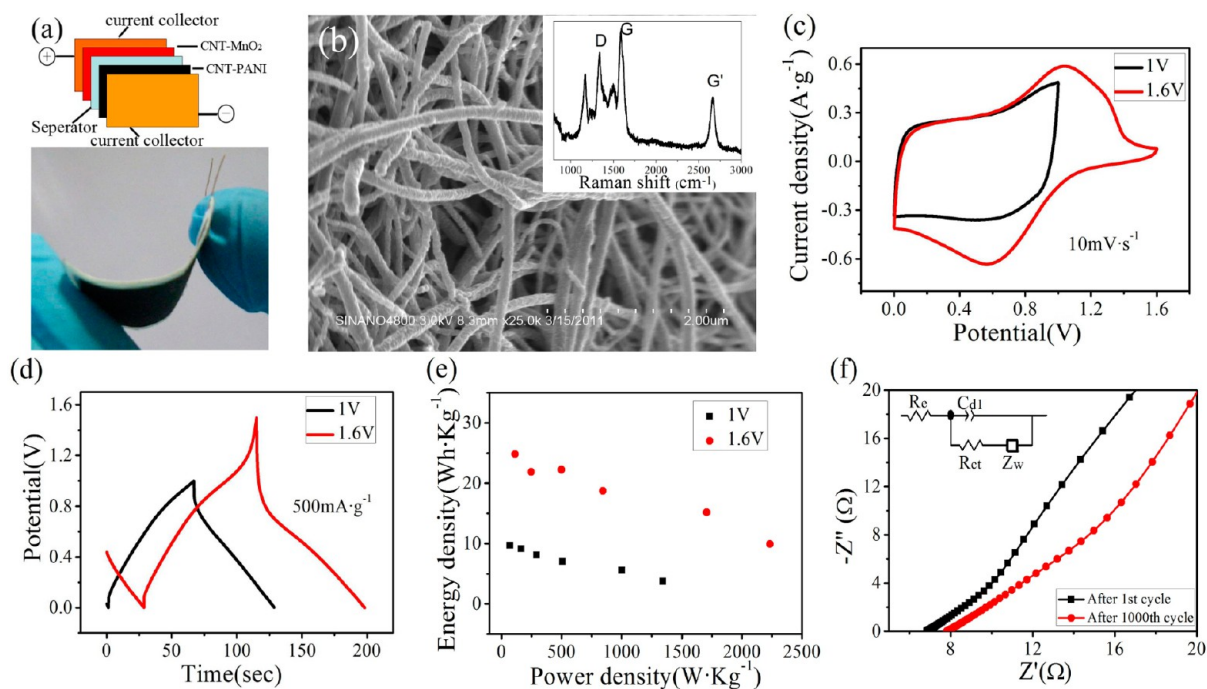
Figure 6. (a) Scheme for assembly structure of asymmetric supercapacitor and its solid flexible device; (b) SEM image of CNT-PANI (inset shows a Raman spectrum); (c) CV curves, (d) charge/discharge curves, (e) Ragone plots of the asymmetric supercapacitor under different potential ranges; and (f) Nyquist plots of the asymmetric supercapacitor before and after 1000 charge/discharge cycles.

CNT/MnO_2 composite paper can dramatically increase the specific capacitance. The pristine CNT paper shows very low specific capacitance of 8 F/g at a scan rate of 2 mV/s, which is due to the raw CNTs with large diameter (50−150 nm), which induced a low specific area (14.1 m^2/g) of the buckypapers, while the electrochemical capacitances of CNT/MnO_2 and $CNT/MnO_2/GR$ could reach 257.8 and 486.6 F/g, respectively (Figure 5c). The Nyquist plots obtained from EIS tests are shown in Figure 5d. The initial nonzero intercept of Z' at the beginning of the semicircle is attributed to the electrical resistance of electrolyte,[26,27] which are ∼3.01, 3.38, and 1.73 Ω for CNT paper, CNT/MnO_2, and $CNT/MnO_2/GR$ in a 1 M Na_2SO_4 electrolyte solution, respectively. The resistance projected by a semicircle is attributed to the electrode materials. Therefore, the charge transfer resistance of CNT paper, CNT/MnO_2, and $CNT/MnO_2/GR$ are 0.403, 20.59, and 7.38 Ω, respectively. This shows an obvious decrease of the charge transfer resistance in CNT/MnO_2 composite paper after GR patching. The charging/discharging cycle life test was used to evaluate the durability of composite paper electrode, which is shown in Figure 5e. After 800 cycles at a current density of 1 A/g, $CNT/MnO_2/GR$ showed good stability and still retained 92.8% of the initial specific capacitance. Comparatively, the specific capacitance of CNT/MnO_2 decreased by 37% under the same condition. This difference in cycle stability between CNT/MnO_2 and $CNT/MnO_2/GR$ can be further revealed by color change in electrolyte solution after cycle tests, as shown in Figure 5f. After charge/discharge cycle for 12 h, the electrolyte solution in CNT/MnO_2 already changed to light brown, which should be attributed to the shedding of MnO_2 nanospheres from CNTs during the process of charge/discharge cycling and crystal shrinkage/expansion, while that in $CNT/MnO_2/GR$ was still colorless. The phenomenon suggests that the patching of GR on the composite paper can effectively prevent the shedding of MnO_2 from the composite electrode in a Faraday

reaction and enhance its cycle stability.[28−30] The GR sheet could be fixed on the surface of the composite paper by frictional forces and van der Waals' forces, and it has no shrinkage/expansion in the process of charge/discharge cycles. These performances ensure that GR does not dissolve into the electrolyte. Therefore, it could form a shell to protect MnO_2 nanospheres.

For future applications, high-performance supercapacitors are expected to be operated with high voltage, high energy density, and long cycle life. An asymmetric supercapacitor is a promising design strategy with high cell voltage and, consequently, high energy density. The flexible CNT paper presents a tailorable substrate to construct a versatile electrode system, based the combination of various chemical active materials. Herein, an asymmetric supercapacitor was assembled by active material modified-CNT paper electrodes, in which $CNT/MnO_2/GR$ composite paper was the positive electrode and CNT/PANI composite paper was chosen as the negative electrode. The structural and electrochemical performance characteristics of the CNT/PANI composite paper were reported by the authors in ref 31. Solid electrolyte gel was prepared by 1 M Na_2SO_4 in PVP solution, which served as the separator in the meantime.[23,32] This composite paper showed enough flexibility and strength to be used directly as electrodes. For the assembly, the positive and negative electrode papers soaked with Na_2SO_4/PVP gel were stacked and pressed together, and sealed by PET thin film. Figure 6a shows the structure scheme and the optical morphology of the flexible device. In the negative system, PANI was electrochemically polymerized around individual CNTs in the CNT paper. SEM image and Raman spectra of CNT/PANI composite paper are shown in Figure 6b. The figure indicates that a continuous PANI coating was formed on the surface of the CNT. The coated PANI is fluffy and shows a porous characteristic. In its Raman spectrum, apart from the D, G, and G′ bands of CNTs, three representative peaks arising from

PANI can be indexed to C−H bending of the quinoid ring at 1173 cm^{-1}, C−H bending of the benzenoid ring at 1233 cm^{-1}, and C−C stretching of the benzene ring at 1502 cm^{-1}, respectively.[33,34]

Specific capacitance, energy density, and power density are the three important performance indicators for supercapacitors. Higher specific capacitance and higher operating voltage will make higher specific energy densities. The electrochemical capacitive performances of the assembled asymmetric supercapacitor were tested. It was found that its operating voltage could be increased to 1.6 V. Figure 6c shows the CV curves of the supercapacitor at a scan rate of 10 mV/s in operating voltages of 1 and 1.6 V, respectively. Their corresponding charge/discharge curves at the current density of 500 mA/g are shown in Figure 6d. The supercapacitor shows a stable Coulombic efficiency (CE) near 100%. Its CE is 96.5% at 0.13 A/g and 96.2% at 5.00 A/g (see Figure S6 in the Supporting Information). Figure 6e shows the Ragone plot of the energy density versus power density considering the total mass of composite papers from positive and negative electrodes. They are calculated by eqs 1, 3, and 4. The maximum energy densities of 24.8 Wh/kg and 9.69 Wh/kg are achieved using this asymmetric supercapacitor at operating voltages of 1.6 and 1 V, respectively. Compared to similar systems reported previously using symmetric MnO$_2$//MnO$_2$,[35] or other hybrid MnO$_2$//carbon-based materials[36−40] (CNTs or active carbon) or MnO$_2$//PEDOT,[41] this asymmetric supercapacitor exhibits comparable energy density. Nyquist plots of the asymmetric supercapacitor over the frequency range of 10^{-2}−10^5 Hz measured during the cycle life tests, and the electrical equivalent circuit used for fitting impedance spectra are shown in Figure 6f. Equivalent series resistance values are ∼6.80 Ω for first cycle and ∼7.76 Ω for the 1000th cycle; this indicates stable electrochemical performance of the supercapacitor in the cyclic test.

4. CONCLUSIONS

In summary, reduced graphene sheet (GR)-patched carbon nanotube (CNT)/MnO$_2$ composite paper shows enhanced specific capacitance, power density, and energy density than the same electrode without GR. It could be attributed to the surface conductivity improvement of the composite paper and the protection of MnO$_2$ nanospheres from detaching with the composite paper and dissolving into the electrolyte. Flexible asymmetric supercapacitor with large power density and energy density was assembled based on these CNT composite paper electrodes, suggesting its prospective application potential in flexible devices.

ASSOCIATED CONTENT

Ⓢ Supporting Information

The study of the MnO$_2$ nanoflowers on CNT paper including SEM images and XPS analysis, the binding performance and rate performance (in CV curves) of the ternary composite electrode, the Coulombic efficiency and self-discharge curve of the asymmetric supercapacitor. This material is available free of charge via the Internet at http://pubs.acs.org.

AUTHOR INFORMATION

Corresponding Author

*Tel./Fax: 86-512-62872552. E-mail addresses: mhchen2008@ sinano.ac.cn (M.H.C.), qwli2007@sinano.ac.cn (Q.L.).

Author Contributions

§These authors contributed equally to this work.

Notes

The authors declare no competing financial interest.

ACKNOWLEDGMENTS

REFERENCES

(1) Nyholm, L.; Nyström, G.; Mihranyan, A. *Adv. Mater.* **2011**, *23*, 3751−3769.

(2) Simon, P.; Gogotsi, Y. *Nat. Mater.* **2008**, *7*, 845−854.

(3) Wang, G.; Zhang, L.; Zhang, J. *Chem. Soc. Rev.* **2012**, *41*, 797−828.

(4) Hall, P. J.; Mirzaeian, M.; Fletcher, S. I.; Sillars, F. B.; Rennie, A. J. R.; Shitta-Bey, G. O.; Wilson, G.; Crudenb, A.; Carterb, R. *Energy Environ. Sci.* **2010**, *3*, 1238−1251.

(5) Sherrill, S. A.; Banerjee, P.; Rubloff, G. W.; Lee, S. B. *Phys. Chem. Chem. Phys.* **2011**, *13*, 20714−20723.

(6) Candelaria, S. L.; Shao, Y.; Zhou, W.; Li, X.; Xiao, J.; Zhang, J.; Wang, Y.; Liu, J.; Li, J.; Cao, G. *Nano Energy* **2012**, *1*, 195−220.

(7) Zhao, X.; Sanchez, B. M.; Dobson, P. J.; Grant, P. S. *Nanoscale* **2011**, *3*, 839−855.

(8) Bailey, M. R.; Donne, S. W. *J. Electrochem. Soc.* **2012**, *159*, A999−A1004.

(9) Song, M. K.; Cheng, S.; Chen, H.; Qin, W.; Nam, K. W.; Xu, S.; Yang, X. Q.; Bongiorno, A.; Lee, J.; Bai, J.; Tyson, T. A.; Cho, J.; Liu, M. *Nano Lett.* **2012**, *12*, 3483−3490.

(10) Wang, J. G.; Yang, Y.; Huang, Z. H.; Kang, F. *Electrochem. Acta* **2011**, *56*, 9240−9247.

(11) Hu, L.; Chen, W.; Xie, X.; Liu, N.; Yang, Y.; Wu, H.; Yao, Y.; Pasta, M.; Alshareef, H. N.; Cui, Y. *ACS Nano* **2011**, *5*, 8904−8913.

(12) Hu, L.; Pasta, M.; Mantia, F. L.; Cui, L. F.; Jeong, S.; Deshazer, H. D.; Choi, J. W.; Han, S. M.; Cui, Y. *Nano Lett.* **2010**, *10*, 708−714.

(13) Yu, G.; Hu, L.; Vosgueritchian, M.; Wang, H.; Xie, X.; McDonough, J. R.; Cui, X.; Cui, Y.; Bao, Z. *Nano Lett.* **2011**, *11*, 2905−2911.

(14) Zhao, Y. Q.; Zhao, D. D.; Tang, P. Y.; Wang, Y. M.; Xu, C. L.; Li, H. L. *Mater. Lett.* **2012**, *76*, 127−130.

(15) Wang, Y. L.; Zhao, Y. Q.; Xu, C. L. *J. Solid State Electrochem.* **2012**, *16*, 829−834.

(16) Wang, N.; Wu, C.; Li, J.; Dong, G.; Guan, L. *ACS Appl. Mater. Interfaces* **2011**, *3*, 4185−4189.

(17) Chou, S. L.; Wang, J. Z.; Chew, S. Y.; Liu, H. K.; Dou, S. X. *Electrochem. Commun.* **2008**, *10*, 1724−1727.

(18) Hou, Y.; Cheng, Y.; Hobson, T.; Liu, J. *Nano Lett.* **2010**, *10*, 2727−2733.

(19) Yu, G.; Hu, L.; Liu, N.; Wang, H.; Vosgueritchian, M.; Yang, Y.; Cui, Y.; Bao, Z. *Nano Lett.* **2011**, *11*, 4438−4442.

(20) Lei, Z.; Shi, F.; Lu, L. *ACS Appl. Mater. Interfaces* **2012**, *4*, 1058−1064.

(21) Hummers, W. S.; Offeman, R. E. *J. Am. Chem. Soc.* **1958**, *80*, 1339.

(22) Li, D.; Muller, M. B.; Gilje, S.; Kaner, R. B.; Wallace, G. G. *Nat. Nanotechnol.* **2008**, *3*, 101−105.

(23) Meng, C.; Liu, C.; Chen, L.; Hu, C.; Fan, S. *Nano Lett.* **2010**, *10*, 4025−4031.

(24) Xiong, Y.; Xie, Y.; Li, Z.; Wu, C. *Chem.—Eur. J.* **2003**, *9*, 1645−1651.

(25) Chigane, M.; Ishikawa, M. *J. Electrochem. Soc.* **2000**, *147*, 2246−2251.

(26) Yang, X.; Zhu, J.; Qiu, L.; Li, D. *Adv. Mater.* **2011**, *23*, 2833–2838.

(27) Kim, C.; Ngoc, B. T. N.; Yang, K. S.; Kojima, M.; Kim, Y. A.; Kim, Y. J.; Endo, M.; Yang, S. C. *Adv. Mater.* **2007**, *19*, 2341–2346.

(28) Zhou, W.; Zhu, J.; Cheng, C.; Liu, J.; Yang, H.; Cong, C.; Guan, C.; Jia, X.; Fan, H. J.; Yan, Q.; Li, C. M.; Yu, T. *Energ. Environ. Sci.* **2011**, *4*, 4954–4961.

(29) Wang, D.; Choi, D.; Li, J.; Yang, Z.; Nie, Z.; Kou, R.; Hu, D.; Wang, C.; Saraf, L. V.; Zhang, J.; Aksay, I. A.; Liu, J. *ACS Nano* **2009**, *3*, 907–914.

(30) Zhou, G. M.; Wang, D. W.; Li, F.; Zhang, L. L.; Li, N.; Wu, Z. S.; Wen, L.; Lu, G. Q.; Cheng, H. M. *Chem. Mater.* **2010**, *22*, 5306–5313.

(31) Jin, Y.; Chen, H.; Chen, M.; Liu, N.; Li, Q. *Acta Phys. Chim. Sin.* **2012**, *28*, 609–614.

(32) Choi, B. G.; Hong, J.; Hong, W. H.; Hammond, P. T.; Park, H. *ACS Nano* **2011**, *5*, 7205–7213.

(33) Louarn, G.; Lapkowski, M.; Quillard, S.; Pron, A.; Buisson, J. P.; Lefrant, S. *J. Phys. Chem.* **1996**, *100*, 6998–7006.

(34) Yan, X. B.; Han, Z. J.; Yang, Y.; Tay, B. K. *Sens. Actuators B* **2007**, *123*, 107–113.

(35) Cottineau, T.; Toupin, M.; Delahaye, T.; Brousse, T.; Belanger, D. *Appl. Phys. A—Mater.* **2006**, *82*, 599–606.

(36) Khomenko, V.; Raymundo-Pinero, E.; Beguin, F. *J. Power Sources* **2006**, *153*, 183–190.

(37) Wu, Z. S.; Ren, W. C.; Wang, D. W.; Li, F.; Liu, B.; Cheng, H. M. *ACS Nano* **2010**, *4*, 5835–5842.

(38) Brousse, T.; Toupin, M.; Belanger, D. *J. Electrochem. Soc.* **2004**, *151*, A614–622.

(39) Fan, Z.; Yan, J.; Wei, T.; Zhi, L.; Ning, G.; Li, T.; Wei, F. *Adv. Funct. Mater.* **2011**, *21*, 2366–2375.

(40) Gao, H.; Xiao, F.; Ching, C. B.; Duan, H. *ACS Appl. Mater. Interfaces* **2012**, *4*, 2801–2810.

(41) Khomenko, V.; Raymundo-Pinero, E.; Frackowiak, E.; Beguin, F. *Appl. Phys. A—Mater.* **2006**, *82*, 567–573.